Electronic structure of self-assembled InAs quantum disks in an axial magnetic field and two-electron quantum-disk qubit

Qing-Rui Dong,[a] Shu-Shen Li, Zhi-Chuan Niu, Song-Lin Feng, and Hou-Zhi Zheng
State Key Laboratory for Superlattices and Microstructures, Institute of Semiconductors, Chinese Academy of Sciences, P. O. Box 912, Beijing 100089, People's Republic of China

(Received 11 December 2003; accepted 14 June 2004)

We have studied the single-electron and two-electron vertically assembled quantum disks in an axial magnetic field using the effective mass approximation. The electron interaction is treated accurately by the direct diagonalization of the Hamiltonian matrix. We calculate the six energy levels of the single-electron quantum disks and the two lowest energy levels of the two-electron quantum disks in an axial magnetic field. The change of the magnetic field strongly modifies the electronic structures as an effective potential, leading to the splitting of the levels and the crossings between the levels. The effect of the vertical alignment on the electronic structures is discussed. It is demonstrated that the switching of the ground-state spin exists between $S=0$ and $S=1$. The energy difference ΔE between the lowest $S=0$ and $S=1$ states is shown as a function of the axial magnetic field. It is also found that the variation of the energy difference between the lowest $S=0$ and $S=1$ states in the strong-B $S=0$ state is fairly linear. Our results provide a possible realization for a qubit to be fabricated by current growth techniques. © *2004 American Institute of Physics*. [DOI: 10.1063/1.1779949]

I. INTRODUCTION

A semiconductor quantum dot (QD) is physically similar to a set of atomic electrons bound to a nucleus, and for this reason, these structures are sometimes termed as "artificial atoms." To extend the atomic analogy further, QDs are considered as "artificial molecules"[1] if they join together. The molecular orbitals of coupled QDs have been investigated theoretically.[2–6] In relevant calculations, Harju *et al.*[6] studied a two-electron QD molecule consisting of two laterally coupled QDs in magnetic field by the direct diagonalization of the Hamilonian matrix, and also designed a qubit by the total spin of the two-electron molecule. Fonseca *et al.*[5] studied stacked pyramids using an effective mass approximation with the influence of strain and piezoelectric potential as local modifications for the conduction-band offset. In experimental investigations[7–9] of coupled QDs, the progress of the "indium-flush"[7] technique produced high-quality vertically stacked quantum disks. The applications of vertically aligned structures are focused on fabricating QD lasers,[10,11] light storage devices,[12] and quantum computers.[13,14] Korkusinski and Hawrylak[15] studied the energy spectrum of the structure mentioned earlier in the adiabatic approximation, the influence of the strain, and the dot separation on the formation of the coupled QD levels.

We employ the transfer-matrix formalism[16] to investigate the electronic structures of the single-electron vertically assembled quantum disks in an axial magnetic field. The effect of the vertical alignment on the electronic structures is discussed Based on these results, the calculation of the double-electron levels is carried out by means of the direct diagonalization of the Hamiltonian matrix. We choose basis functions different from those in Ref. 6. These basis functions can provide a more explicit physical sense and reduce the amount of calculation. In the calculation, the electron correlations are treated accurately. These correlation effects are significant for they can lead to the switching of the ground-state spin between $S=0$ and $S=1$, which realizes a qubit of a quantum computer. Our results show that the variation of the energy difference ΔE between the lowest $S=0$ and $S=1$ states is rather linear for the $S=0$ ground state at a larger B. This is remarkably different from the results in Ref. 6. Since the high-quality vertically stacked quantum disks can now be fabricated,[7] it is very realistic to obtain the qubit of this type.

II. ELECTRONIC STRUCTURES OF SINGLE-ELECTRON QUANTUM DISKS

Figure 1 shows two vertically assembled disk-shaped InAs QDs. Each disk grows on a wetting layer (WL) of thickness W containing the GaAs barrier material. Both quantum disks have, the same height H (typically 1–2 nm) and the same radius R (typically 7–12 nm). The distance between the two wetting layers, D, forms a quantum tunneling barrier of thickness $D-H$, and the conduction-band offset between the quantum disks and the surrounding material

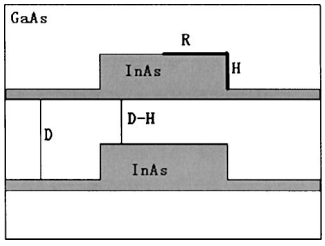

FIG. 1. Schematic of the InAs/GaAs double self-assembled quantum disks of radius R, heights H, and wetting-layer separation D.

[a]Electronic mail: qrdong@red.semi.ac.cn

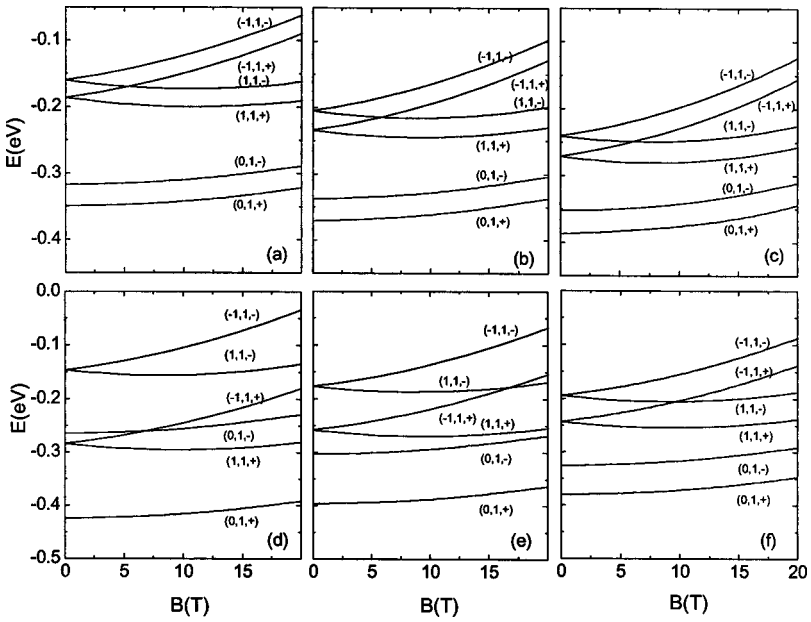

FIG. 2. Six single-electron energies as functions of the magnetic field B. (a) $R=7$ nm, (b) $R=8$ nm, (c) $R=9$ nm, (d) $D=4.5$ nm, (e) $D=5.5$ nm, and (f) $D=6.5$ nm. The figures are plotted for the same $D=7.5$ nm in (a), (b), and (c), whereas the same $R=12$ nm is used in (d), (e), and (f). States are labeled by their angular momentum, radial quantum number, and isospin. All states are on the lowest levels before $B \approx 8$ T.

forms the confining potential V_0 for the quantum disks. The material parameters of the quantum disks and the WLs have their effects through the effective Rydberg $R=m_e e^4/2\epsilon^2\hbar^2$ and the effective Bohr radius $a_B=\epsilon\hbar^2/m_e e^2$, where m_e and ϵ are the effective mass of an electron and the dielectric constant, respectively. Throughout this paper, we will use R and a_B as the units of energy and length, respectively.

In the effective mass approximation, the Schrödinger equation for one electron in cylindrical coordinates is expressed as

$$\hat{H}\psi(r,\theta,z) = E\psi(r,\theta,z), \tag{1}$$

where

$$\hat{H} = -\frac{1}{r^2}\left(r\frac{\partial}{\partial r}r\frac{\partial}{\partial r} + \frac{\partial^2}{\partial\theta^2}\right) + \frac{eB}{c}l_z + \frac{e^2B^2}{4c^2}r^2 - \frac{\partial^2}{\partial z^2} + V(r,z), \tag{2}$$

with the potential $V(r,z)=-V_0$ inside the WL and the quantum disks, and $V(r,z)=0$ in the barrier. Because the height of both quantum disks is much smaller than their radius, the electron motion in the growth direction is strongly confined. In an adiabatic approximation, the wave function is written as $(1/\sqrt{2})e^{im\theta}g_r^v(z)f_m^v(r)$. In the growth direction, the structure includes two identical quantum wells, whose widths are $H+W$ or W. The ground-state energy of each isolated well is denoted by E_0, and the corresponding wave functions of the two isolated wells are denoted by $g_1(z)$ and $g_2(z)$. The wave function $g_r^0(z)$ can be expressed in the form of symmetric and asymmetric linear combinations of the individual quantum well orbitals: $g_s^0(z)=[g_1(z)+g_2(z)]/2$ and $g_{as}^0(z)=[g_1(z)-g_2(z)]/2$; the corresponding eigenenergies are $E_s=E_0-\Delta/2$ and $E_{as}(z)=E_0+\Delta/2$, respectively, with Δ being the splitting between these levels. While the motion in the plane of the disk is quantized, the radial wave function corresponds to the Bessel functions. For infinite barriers, the lateral spectrum can be written in terms of zeros of the Bessel function $\alpha_m^n: E(m,n)=(\alpha_m^n/R)^2$, where R is the radius of the disk, n is the radial quantum number, and m is the angular momentum. Therefore, the electronic spectrum of the structure is composed of two ladders of states: the symmetric one, $E_0-\Delta/2+E(0,1),\ldots$, labeled as $(m,n,+)$; and the antisymmetric one, $E_0+\Delta/2+E(0,1),\ldots$, labeled as $(m,n,-)$. For each angular momentum channel m, the functions $g_r^v(z)$ and $f_m^v(r)$ satisfy the following set of equations:

$$\left[-\frac{\partial^2}{\partial z^2} + V(r,z)\right]g_r^v(z) = E_v(r)g_r^v(z), \tag{3}$$

$$[\hat{H}_R + E_v(r)]f_m^v(r) = Ef_m^v(r). \tag{4}$$

$$\hat{H}_R = -\frac{1}{r^2}\left(r\frac{\partial}{\partial r}r\frac{\partial}{\partial r} - m^2\right) + \frac{eB}{c}l_z + \frac{e^2B^2}{4c^2}r^2. \tag{5}$$

We first find the energy $E_v(r)$ corresponding to that of the motion in the growth direction for a given set of structure parameters. The details of the computational procedure can be found elsewhere.[15] Because $[eBl_z/c,\hat{H}_R]=0$, Eq. (4) shares the same eigenfunctions with the following equation:

$$\left[-\frac{1}{r^2}\left(r\frac{\partial}{\partial r}r\frac{\partial}{\partial r} - m^2\right) + \frac{e^2B^2}{4c^2}r^2 + E_v(r)\right]f_m^v(r) = E'f_m^v(r). \tag{6}$$

The radial wave function $f_m^v(r)$ is solved for each angular momentum channel. We approximate the effective potential $e^2B^2r^2/4c^2+E_v(r)$ by the n-step piecewise potential: $V(r)=v_i$, if $r_i \leqslant r \leqslant r_{i+1}$, where $0 \leqslant i \leqslant n, r_0=0$, $r_{i+1}=r_i+\Delta r$, Δr being the step length. By using the transfer-matrix formalism, E' and $f_m^v(r)$ can be obtained. The total energy of the system is

$$E = E' \mp \frac{eB}{c}m\hbar. \tag{7}$$

In addition, the wave function $(1/\sqrt{2})e^{im\theta}g_r^v(z)f_m^v(r)$ is obtained and will be used as a basis function afterwards.

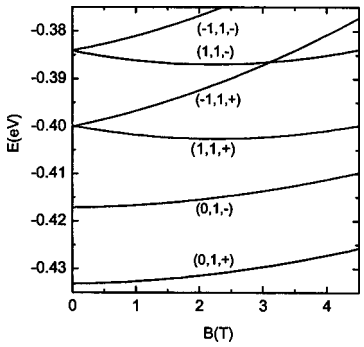

FIG. 3. The dependence of the electronic structures on the axial magnetic field B, with $H=2$ nm, $R=19$ nm, and $D=9$ nm.

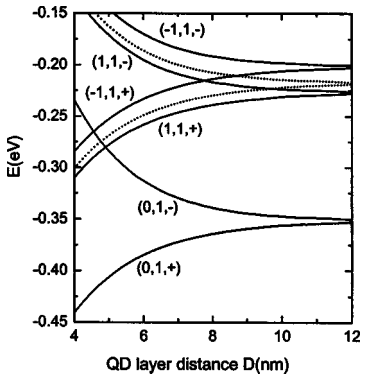

FIG. 4. The dependence of the electronic structures on the wetting-layer spacing D, with the magnetic field $B=5$ T, $H=2$ nm, and $R=12$ nm. The dotted lines are for the situation without magnetic field.

Figure 2 shows the dependence of the electronic states on the axial magnetic field B. The six states are presented with the disk height $H=2$ nm, the confining potential $V_0=1$ eV, corresponding to the band offset between InAs and GaAs, and the effective mass $m_e=0.23;m_0$ for unstrained InAs.

In Fig. 2, we show the electronic states for three different disk radii: (a) $R=7$ nm, (b) $R=8$ nm, and (c) $R=9$ nm. As the radius becomes larger, the quantum confinement is weaker, which makes every level lower. At $B=0$, the states $(-1,1,+)$ and $(1,1,+)$ become degenerate and the states $(-1,1,-)$ and $(1,1,-)$ get degenerate too. With increasing magnetic field, the states with positive and negative angular momenta split. The splitting depends linearly on B and results in a crossing of the states $(-1,1,+)$ and $(1,1,-)$. The states $(0,1,\pm)$ get higher with B due to the effective potential $e^2B^2r^2/4c^2$. As the magnetic field becomes stronger, the effective potential $e^2B^2r^2/4c^2$ also becomes more important, which can be understood easily from the fact that the levels $(1,1,\pm)$ reverse the trend of getting lower with B, because the effective potential $e^2B^2r^2/4c^2$ makes all levels higher. In Figs. 2(d)–2(f), the electronic states for three different distances D between two quantum disks are plotted. The results show that as D decreases, the splitting of the symmetric and the asymmetric states enhances. In Fig. 2(d), the level $(0,1,-)$ is higher than the levels $(\pm,1,+)$ at $B=0$, but the level $(-1,1,+)$ will exceed the level $(0,1,-)$ with increasing B; on the other hand, the level $(1,1,+)$ remains lower than the level $(0,1,-)$.

To compare the effect of the vertical alignment on the electronic structures with that of the lateral alignment in Ref. 6, we show the electronic structure with $R=19$ nm in Fig. 3. In Ref. 6. the confinement strength $\hbar\omega_0=3.0$ meV is provided by the quantum dot with $R=19$ nm for $\langle 0|r^2|0\rangle=\hbar/(2m\omega_0)$ is roughly equal to the dot size (radius of the cylinder) in the radial direction. This is the reason why we choose $R=19$ nm in the present calculation. Here, $|0\rangle$ indicates the ground state. The coupling of the two QDs is due to the superposition of the vertical wave functions in Ref. 6, whereas in the present calculation, the coupling of the two QDs is due to the superposition of the radial wave functions. Because the two QDs in the vertical alignment are identical, the "symmetric" and "antisymmetric" levels can be distinguished for each angular momentum. The two QDs in the lateral alignment do not posses translation symmetry in the lateral direction: thus, there exist no pairs of symmetric and antisymmetric levels. Moreover, because there is no rotation invariance in the system in the lateral alignment, the angular momentum is not a conserved quantity. The level of symmetry in the vertical alignment is higher than that in the lateral alignment.

In addition, we investigate the dependence of the electronic states on the wetting-layer spacing D (see Fig. 4). In contrast to the situation without the magnetic field, the Zeeman term leads to the splitting between the level $(-1,1,-)$ and the level $(1,1,-)$, as well as the splitting between the level $(-1,1,+)$ and the level $(1,1,+)$. There are some crossing of states with different angular momenta, but the origins that lead to their crossings are different. As the spacing D decreases, for each angular momentum the splitting between the "symmetric" and "antisymmetric" levels increases. When the splitting exceeds the quantization of the radial motion, the crossing between the level $(0,1,-)$ and the level $(1,1,+)$ occurs. Whereas the occurrence of the crossing between the levels $(1,1,-)$ and $(-1,1,+)$ is due to the fact that the splitting exceeds the difference of their Zeeman terms.

III. ELECTRONIC STRUCTURES OF TWO-ELECTRON QUANTUM DISKS AND TWO-ELECTRON QUANTUM-DISK QUBIT

In the following, we investigate the variation of the two-electron levels of vertically assembled quantum disks vs the axial magnetic field. The spin-free Hamiltonian of the system can be expressed as

$$\hat{H}=\hat{H}_1+\hat{H}_2+\frac{e^2}{\epsilon r_{12}}, \tag{8}$$

where $\hat{H}_1$ and $\hat{H}_2$ are single-electron Hamiltonians of the system and remain in the formalism of Eq. (1). The Zeeman coupling $E_z=g^*\mu_B BS_z$ of the magnetic field to S_z can be taken into account afterwards. We have obtained numerically the eigenstates of the single-electron part of Eq. (8), $\psi(r,\theta,z)=(1/\sqrt{2})e^{im\theta}g_r^v(z)f_m^v(r)$; thus, two-electron wave function with the total spin S can be expressed as

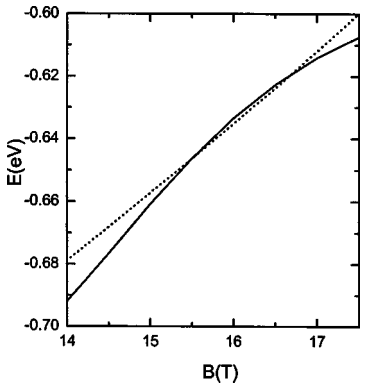

FIG. 5. The two lowest two-electron states vs the axial magnetic field B, with $H=2$ nm, $D=7.5$ nm, and $R=12$ nm. The solid line is for the $S=0$ state, and the dotted line is for the $S=1$ state.

$$\psi_S(r_1,r_2)=\sum_{i\leqslant j}\alpha_{i,j}\{\psi_i(r_1,\theta_1,z_1)\psi_j(r_2,\theta_2,z_2) + (-1)^S\psi_i(r_2,\theta_2,z_2)\psi_j(r_1,\theta_1,z_1)\}, \quad (9)$$

which is symmetric for $S=0$ and antisymmetric for $S=1$. The spin part of the wave function is not explicitly written, so we still work with the spin-independent wave functions in the following. The coefficient vector α_i and the corresponding energy E_l for the lth eigenstate are found from a generalized eigenvalue problem, in which the Hamiltonian matrix elements can be calculated numerically. Choosing the single-electron states as basis functions, which are different from those in Ref. 6. the matrix elements corresponding to $\hat{H}_1$ and $\hat{H}_2$ can be achieved directly. By changing the number of basis functions, we can check the convergence and find that it is sufficient for obtaining the two lowest double-electron states by using the four single-electron states $(0,1,\pm)$ and $(\pm1,1,+)$ as the basis functions. This can be explained simply by the fact that the two double-electron states are mainly composed of the four single-electron states when the wave functions are expanded according to Eq. (9). Moreover, more double-electron states can be achieved by choosing more single-electron states as basis functions.

Figure 5 shows the dependence of the two lowest states on the axial magnetic field B in the range of $B=14 \sim 17.5$ T at $H=2$ nm, $R=12$ nm, and $D=7.5$ nm. The two lowest states possess different spins $S=1$ and $S=0$. When $B=14$ T, in fact, beginning from $B=0$ T, the $S=0$ state is lower than the $S=1$ state. As the magnetic field B enhances, the two lowest double-electron states approach each other. At $B=15.5$ T, the $S=1$ state turns out to be the lower one. At $B=16.8$ T, the $S=0$ state becomes the lower one again. We can explain these transitions by the dependence of the single-electron states on the magnetic field. The two double-electron states are composed mainly of the single-electron states $(0,1,+)$ and $(1,1,+)$. As the magnetic field becomes stronger, the states $(0,1,+)$ and $(1,1,+)$ approach each other. Similarly, the two lowest two-electron states approach each other with increasing magnetic field. If we do not take into account the electron-interaction effects, the $S=0$ state should remain lower forever, because the two electrons of the $S=0$ state occupy the lowest single-electron state, and the two electrons of the $S=1$ state cannot occupy the lowest single-electron state simultaneously according to the Pauli exclusion principle. Due to the effect of the interaction between the two electrons, the difference of the interaction energy between the two states leads the state $S=1$ to become lower than the state $S=0$ at some point, and thus the transition occurs. Now, we consider the effect of the Zeeman term on the energy levels. The energy of the $S=1$ state is lowered by about 60 μeV/T, and that of the $S=0$ state is unaltered. According to the order of the energy levels, the Zeeman term can be neglected.

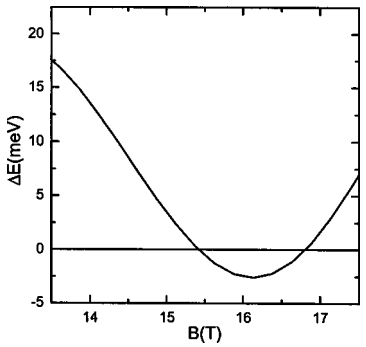

FIG. 6. Energy difference between triplet and singlet states, ΔE, as a function of the magnetic field B with the structures parameters $H=2$ nm, $R=12$ nm, and $D=7.5$ nm.

The energy difference ΔE between the lowest $S=0$ and $S=1$ states is plotted in Fig. 6 at $H=2$ nm, $R=12$ nm, and $D=7.5$ nm. One can obtain different regions of $S=0$ and $S=1$ ground states by changing the structure parameters. The ground-state spin of the double-electron system is either $S=0$ or $S=1$, and we can change the spin by changing the intensity of the axial magnetic field (see Fig 6). The transition from the $S=0$ state to the $S=1$ state allows us to use the total spin of the system as a qubit. However, it should be noted that there is a remarkable difference between our present calculation and that in Ref. 6. In Ref. 6, when the external magnetic field becomes stronger, it will be difficult to distinguish the lowest $S=0$ state from the lowest $S=1$ state, and this removes the possibility to use the strong B states for making a qubit. The little energy difference of the lowest $S=0$ and $S=1$ states can be explained by the fact that the single-electron levels are very close to each other in a strong external magnetic field. However, the single-electron levels of vertically assembled quantum disks do not approach each other but interest each other. Thus, in our result, the variation of ΔE in the strong-B $S=0$ state is fairly linear, suggesting that the strong-B states can be used for making a qubit. Because the confining potential is stronger, the size of the quantum dots is smaller and material parameters are different in the present system, the maximum energy difference ΔE in the $S=1$ state is at least ten times as large as that in Ref. 6. Since high-quality vertically stacked quantum disks can now be fabricated, the significance of the present calculation lies in that it is realistic beyond a model.

IV. CONCLUSION

In conclusion, we have calculated the electronic structures of vertically assembled quantum disks as a function of

the axial magnetic field. The electronic structures are determined by the combined effect of the quantum confinement and the magnetic field. The total spin of the two-electron ground state of the system can be changed by adjusting the magnetic field between $S=0$ and $S=1$. The variation of the energy difference between the lowest $S=0$ and $S=1$ states in the strong-B $S=0$ state is fairly linear like that of the week-B $S=0$ state. The results support the possibility to use the system we studied as a qubit of a quantum computer, which can be fabricated by current growth techniques.

ACKNOWLEDGMENTS

This work was supported by the National Natural Science Foundation of China and the Special Foundation for State Major Basic Research Program of China (Grant No. G2001CB309500).

[1]M. A. Kastner, Phys. Today **46**, 24 (1993).
[2]J. J. Palacios and P. Hawrylak, Phys. Rev. B **51**, 1769 (1995).
[3]Y. Tokura, D. G. Austing, and S. Tarucha, J. Phys.: Condens. Matter **11**, 6023 (1999); G. W. Bryant, Phys. Rev. B **47**, 1683 (1993).
[4]C. Pryor, Phys. Rev. Lett. **80**, 3579 (1998).
[5]L. R.C. Fonseca, J. L. Jimenez, and J. P. Leburton, Phys. Rev. B **58**, 9955 (1998).
[6]A. Harju, S. Siljamaki, and R. M. Nieminen, Phys. Rev. Lett. **88**, 226804 (2002).
[7]Z. R. Wasilewski, S. Fafard, and J. P. McCaffrey, J. Cryst. Growth **201**, 1131 (1999).
[8]R. H. Blick, D. Pfannkuche, R. J. Haug, K. V. Klitzing, and K. Eberl, Phys. Rev. Lett. **80**, 4032 (1998).
[9]R. J. Luyken, A. Lorke, M. Fricke, J. P. Kotthaus, G. Mederios-Ribeiro, and P. M. Petroff, Nanotechnology **10**, 14 (1999).
[10]M. V. Maximo *et al.*, J. Appl. Phys. **83**, 5561 (1998).
[11]S. Fafard, Z. R. Wasilewski, C. Ni. Allen, K. Hinzer, J. P. MoCaffrey, and Y. Feng, Appl. Phys. Lett. **75**, 986 (1999).
[12]T. Lundstrom, W. Schoenfeld, H. Lee, and P. M. Petroff, Science **286**, 2312 (1999).
[13]P Hawrylak, S. Fafard and Z. R. Wasilewski, Condens. Matter News **7**, 16 (1999)
[14]G. Burkard, G. Seelig, and D. Loss, Phys. Rev. B **62**, 2581 (2000).
[15]M. Korkusinski and P. Hawrylak, Phys. Rev. B **63**, 195311 (2001).
[16]A. Wojs, P. Hawrylak, S. Fafard, and L. Jacak, Phys. Rev. B **54**, 5604 (1996).